Int. J. Heat Mass Transfer. Vol. 34, No. 12, pp. 3037–3046, 1991
Printed in Great Britain

0017–9310/91 $3.00+0.00

Analysis of natural convection in vertically-vented enclosures

D. M. SEFCIK, B. W. WEBB and H. S. HEATON
Heat Transfer Laboratory, Brigham Young University, Provo, UT 84602, U.S.A.

(*Received* 16 *October* 1990 *and in final form* 12 *February* 1991)

Abstract—Natural convection in vertically-vented enclosures is investigated theoretically. A vertically-vented enclosure is one in which the buoyancy-driven flow and heat transfer are restricted by vents in the top and bottom bounding walls of the enclosure. The governing conservation equations are solved numerically using a control volume-based finite difference technique with the appropriate pressure boundary conditions at the inlet and exit vents. The results reveal strongly non-uniform local heat transfer along the isothermal wall as a result of the blockage at the inlet. A local maximum and minimum in heat transfer occur in the lower half of the enclosure. The predictions for the flow field reveal that these heat transfer extrema are attributed to a recirculation zone near the inlet gap and primary flow attachment along the heated wall. The results show asymptotic behavior to the classical vertical parallel plate result in the limit as the vent gap approaches the enclosure width.

INTRODUCTION

NATURAL convection cooling is frequently encountered in electronic cooling applications. Passive (natural convective) cooling is still the preferred thermal control technique due to its low cost and maintenance, and absence of electromagnetic interference. In many passive cooling situations the heat sources are mounted on arrays of vertically-configured boards. The entrance and exit of the vertical channels formed by these arrays may be purposely obstructed as a protection against hostile or dirty environments. The situation is then one of natural convection in a vertically-vented enclosure with one vertical wall heated and the opposite vertical wall adiabatic. The vertical venting designation indicates that the buoyancy-driven flow and heat transfer are restricted by vents of variable dimension in the top and bottom bounding walls of the enclosure, as shown in the schematic of Fig. 1.

When the gap spacing is increased so that it is equal to the width of the enclosure, the vertically-vented enclosure becomes an asymmetrically-heated, vertical parallel plate channel. Such a configuration has been studied extensively both numerically and experimentally [1–3]. A thorough review of previous work on natural convection in parallel plate channels may be found in ref. [4]. Buoyancy-driven flow and heat transfer in fully or partially open enclosures have also been topics of current research [5–11]. These studies have focused on the transport characteristics of rectangular enclosures heated on one vertical wall with the other vertical boundary being open (or partially open).

Little research exists in the area of natural convection heat transfer in vertically-vented enclosures. The purpose of this study was to analyze the flow and heat transfer in a vertically-vented enclosure containing one isothermally heated wall. This problem is approached with analytical methods. Predictions were obtained by solving numerically the elliptical, partial differential equations which govern the flow and heat transfer over a wide range of the governing dimensionless parameters.

ANALYSIS

The flow through the enclosure and the heat transfer from the isothermal wall were modeled analytically. The partial differential equations governing conservation of mass, momentum, and energy were discretized and solved using a numerical algorithm. The dimensionless equations which govern laminar, buoyancy-driven flow for a Boussinesq fluid are:

continuity

$$\frac{\partial U}{\partial X}+\frac{\partial V}{\partial Y}=0; \tag{1}$$

X-momentum

$$U\frac{\partial U}{\partial X}+V\frac{\partial U}{\partial Y}=-\frac{\partial P}{\partial X}+\frac{\partial^2 U}{\partial X^2}+\frac{\partial^2 U}{\partial Y^2}; \tag{2}$$

Y-momentum

$$U\frac{\partial V}{\partial X}+V\frac{\partial V}{\partial Y}=-\frac{\partial P}{\partial Y}+\frac{\partial^2 V}{\partial X^2}+\frac{\partial^2 V}{\partial Y^2}+Gr\,\theta; \tag{3}$$

energy

$$U\frac{\partial \theta}{\partial X}+V\frac{\partial \theta}{\partial Y}=\frac{1}{Pr}\left(\frac{\partial^2 \theta}{\partial X^2}+\frac{\partial^2 \theta}{\partial Y^2}\right). \tag{4}$$

These equations were solved according to the following boundary conditions. The side wall opposite

NOMENCLATURE

B	length of vent inlet and exit vents, Fig. 1
G	width of inlet and exit vent gaps, Fig. 1
H	height of enclosure, Fig. 1
Gr	Grashof number, $g\beta(T_w-T_0)W^3/\nu^2$
k	thermal conductivity
Nu	local Nusselt number along heated wall, $qW/k(T_w-T_0)$
$\overline{Nu}$	average Nusselt number
p_0	local ambient hydrostatic pressure
P	dimensionless pressure defect, $(p-p_0)/\rho(\nu/W)^2$
Pr	Prandtl number, ν/α
q	local convective heat flux along heated wall
T_0	fluid inlet temperature
T_w	isothermal heated wall temperature
(U, V)	dimensionless velocities, $(u, v)W/\nu$
$\bar{v}_{in}$	dimensional average velocity in inlet and exit vent gaps, $\int_{gap} v\,dx/G$
$\bar{V}_{in}$	dimensionless average velocity in inlet and exit vent gaps, $\bar{v}_{in}W/\nu$
W	width of the enclosure, Fig. 1
(X, Y)	dimensionless coordinates, $(x, y)/W$.

Greek symbols

β	volumetric coefficient of thermal expansion
θ	dimensionless temperature, $(T-T_0)/(T_w-T_0)$
ν	kinematic viscosity
ρ	fluid density
ψ^*	dimensionless stream function, ψ/ν.

the heated wall, and the top and bottom walls were considered adiabatic. The heated wall was regarded as isothermal. No-slip hydrodynamic boundary conditions were imposed along all walls of the enclosure. Pressure boundary conditions $P = -\bar{V}_{in}^2/2$ and 0 were imposed at the entrance of the lower vent and the exit of the upper vent, respectively. The solid regions above and below the cavity, adjacent to the inlet and exit vents were considered adiabatic.

Chimney problems, such as the parallel-plate vertical channel configuration, have traditionally been solved numerically using a parabolic scheme [1]. Sufficient information is provided at the inlet and the solution marches forward until the end of the channel is reached. In most cases, an initial velocity at the inlet is given and the marching solution proceeds axially until the pressure defect vanishes. This point defines the channel length corresponding to the imposed inlet velocity. Alternatively, for a specified channel length, the inlet velocity is guessed and the marching solution proceeds to the specified length. If the resulting pressure defect is not identically zero at the channel exit, the inlet velocity is updated and the marching solution procedure is carried out again. The sequential inlet velocity updating procedure is performed iteratively until the pressure at the channel exit is equal to the pressure of the local ambient fluid ($P = 0$).

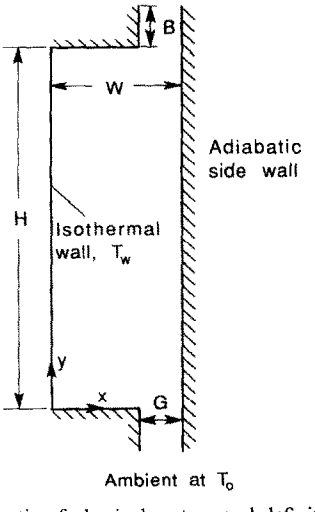

FIG. 1. Schematic of physical system and definition of geometric parameters.

It was not possible to employ a marching scheme to generate a solution for the vertically-vented enclosure since the presence of recirculating flow renders the problem elliptic. Thus, an elliptic numerical scheme was adopted for the solution of the equations. Pressure boundary conditions were imposed at the inlet and exit vent gaps. The pressure at the entrance of the lower vent gap was considered to be uniform and equal to that of the local (entrance elevation) ambient fluid pressure less the dynamic pressure, $P = -\bar{V}_{in}^2/2$, due to the acceleration of stagnant ambient fluid into the cavity [12, 13]. The pressure at the exit of the upper vent gap was also considered to be uniform and equal to the local (exit elevation) ambient fluid ($P = 0$). The governing partial differential equations were then solved using a control volume-based finite difference method. The SIMPLER algorithm was used to treat the coupling between momentum and continuity [14]. The control volume-based solution scheme used proceeds to a converged solution through a series of continuity-satisfying iterations at all internal control volumes. However, since known pressures were imposed at the inlet and exit vents, the velocity distribution at these boundaries were an outcome of the solution. The inlet and exit velocity profiles were determined from a consideration of local continuity at the boundary control volumes. The pressure uniformly imposed at the inlet vent was based on the

current iterative estimate of the average inlet velocity, $\bar{V}_{in}$, and was updated as the iterations proceeded.

A non-uniform grid was used within the enclosure cavity which clustered the majority of the nodes near the bottom of the heated wall. Since the convecting medium was expected to undergo little change in the inlet and exit vents, a relatively coarse uniform grid was utilized in these regions. The number of nodes placed within the inlet and exit channel was varied as the vent gap spacing was changed. Generally, a 10×5 (horizontal $\times$ vertical) grid was used inside each vent gap for a normalized gap spacing $G/W \leqslant 0.33$. As a result, a 52×67 non-uniform grid was utilized within the cavity proper for $G/W \leqslant 0.33$. As G/W was increased, a correspondingly higher number of nodes in the x-direction were added in the inlet and exit vents.

As a check on the methodology using imposed pressures at the inlet and exit vent, a second solution technique was employed. This technique was similar to that described previously for the parabolic (marching) solution of natural convection in unobstructed parallel plates of specified length. A uniform velocity at the inlet vent was guessed. Equations (1)–(4) were then solved to convergence subject to this imposed velocity boundary condition. The average pressure at the exit vent in the converged solution was then examined to determine if the $P = 0$ pressure boundary condition was satisfied. If not, a new inlet velocity was imposed and the governing equations were again solved. The inlet velocities were updated using the secant method via a series of steady-state simulations taken to convergence. The correct inlet velocity was that which yielded a solution whose average pressure at the exit of the upper vent gap was equal to that of the local ambient fluid ($P = 0$). Strict convergence was required during the simulation for each inlet velocity iterate, since the predicted pressure at the exit was quite sensitive to small changes in the specified value of $\bar{V}_{in}$. As expected, this procedure proved to be very computationally intensive.

A comparison of the solution techniques described above was undertaken to assess the possible differences in predicted heat transfer. Predictions for the local Nusselt number profiles, using the iterative inlet velocity boundary condition and the imposed pressure boundary condition, were examined for $H/W = 5.0$, $G/W = 0.33$, and $Gr = 2.2(10^5)$. Excellent agreement was evident for the predictions using the two methods with a maximum variation of 15% in local Nusselt number along the heated wall [15]. The difference in average Nusselt number was found to be less than 3% between the two solution methodologies. The slight variation in predictions is due to the different boundary conditions employed at the inlet. The uniform pressure boundary condition implies a parabolic or fully developed velocity profile at the entrance of the inlet vent. By contrast, the imposed velocity boundary condition iterates on the magnitude of a *uniform* imposed inlet velocity until the exit pressure is equal to the pressure of the local ambient fluid. The pressure boundary condition approach was utilized for this study primarily because of the reduction in the required computing time. More details of the solution techniques and the comparison may be found elsewhere [15].

Grid sizes of 42×52, 52×62, 62×72, and 72×82 were investigated to determine the resolution needed to yield a grid-independent solution. Several configurations were solved using these varying grids and the change in the average Nusselt number and the profiles of the local Nusselt number was monitored. The results of the grid size study are shown in Table 1. As the resolution of the grid was increased above the 62×72 grid, the predictions for $\overline{Nu}$ differed by less than 0.2% for both small and large aspect ratio enclosures. Thus it was determined that a 62×72 grid size yielded a comfortable compromise between grid resolution and required computing time.

The dimensionless stream function is defined based on the customary dimensional counterpart

$$U = \frac{\partial \psi^*}{\partial Y} \tag{5}$$

$$V = -\frac{\partial \psi^*}{\partial X}. \tag{6}$$

The dimensionless stream function ψ^* was obtained from the converged velocity field solution by integrating equations (5) and (6), yielding the pair of equations

$$\psi^*_{X,Y=0} = \psi^*_{X=0,Y=0} - \int_0^X V \, dX \tag{7}$$

$$\psi^*_{X,Y} = \psi^*_{X,Y=0} + \int_0^Y U \, dY \tag{8}$$

where $\psi^*_{X=0,Y=0}$ was taken arbitrarily to be zero.

RESULTS AND DISCUSSION

The model was evaluated by comparison with experimental data. The details of the model verification will first be presented, followed by results of a numerical study investigating the influence of the dimensionless parameters on flow and transport in the vertically-vented enclosure.

Model verification

The analytical model presented in the foregoing was validated by comparison with experimental data. An enclosure was constructed with attributes shown in the schematic of Fig. 1. The heated wall was maintained at a constant temperature by circulating thermally-regulated fluid through a copper plate with counter-current channels milled in its interior. Multiple thermocouples embedded in the copper plate ensured an isothermal boundary. The remaining walls were maintained nearly adiabatic by constructing

Table 1. Predicted average Nusselt number as a function of grid size used

Test case conditions			Predicted average Nusselt number			
H/W	G/W	Gr	42×52	52×62	62×72	72×82
10	0.67	$2.9(10^4)$	3.49	3.50	3.50	3.50
5.0	0.20	$2.2(10^5)$	5.70	5.72	5.73	5.74
2.5	0.33	$1.8(10^6)$	12.49	12.46	12.45	12.44
5.0	0.33	$3.0(10^5)$	6.33	6.37	6.39	6.38
1.88	0.33	$4.3(10^6)$	16.14	16.15	16.04	16.07

them of closed-pore extruded polystyrene. Movable horizontal boundaries constructed of balsa wood enabled the inlet and exit vent gaps to be changed. Optical quality glass was placed at the spanwise ends of the enclosure. This allowed optical access to the convecting air medium for Mach–Zehnder interferometric studies. The height of the heated wall, H, was maintained constant at 19.05 cm, while the width of the enclosure, W, was varied from 1.91 to 10.2 cm. The gap spacing was adjusted through a range of 1.91 mm to 10.2 cm. The length of the inlet and exit vent, B, was held constant at 5.08 cm. The spanwise dimension of the enclosure was 30.5 cm. Local heat transfer from the isothermal wall was measured experimentally from isotherms using a Mach–Zehnder interferometer (MZI) with 30.5 cm optics. The local heat transfer was measured at approximately 25 locations along the isothermal wall. Average Nusselt number data were determined by the appropriate integration of the local heat transfer profiles. This provided data for the evaluation of the numerical model. More details of the apparatus and the experimental results may be found elsewhere [15].

Figure 2 illustrates the predicted and experimentally-determined local heat transfer profiles along the heated wall for two test cases: $H/W = 5.0$, $G/W = 0.2$, $Gr = 2.17(10^5)$; and $H/W = 10.0$, $G/W = 0.67$, $Gr = 2.89(10^4)$. The model predicts quite well both trends and magnitude of the local heat transfer. The analytical solutions were found to predict the average Nusselt number, $\overline{Nu}$, to within 8% of the experimental data for the two cases shown. Numerical simulation of other configurations studied experimentally revealed a maximum deviation of model predictions from data of 15% except for the $G/W = 0.10$ gap spacing, where the predicted $\overline{Nu}$ was 31% lower than the experimentally obtained value [15]. The large difference was attributed primarily to the high fractional uncertainty in the measurement of the gap spacing for the experimental enclosure, since $G = 3.8$ mm only for the $G/W = 0.1$ configuration. The heat transfer profile was found to be highly sensitive to the size of the inlet for small spacings. This will be borne out by parametric calculations to be presented.

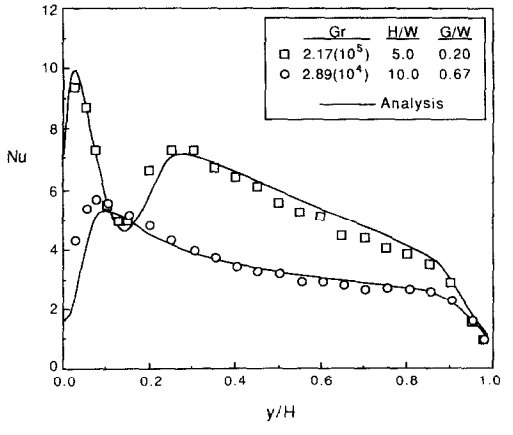

FIG. 2. Comparison of predicted and experimentally-determined local Nusselt numbers for $H/W = 5.0$, $G/W = 0.2$, $Gr = 2.17(10^5)$, and $H/W = 10.0$, $G/W = 0.67$, $Gr = 2.89(10^4)$.

Parametric study

A parametric study which included the investigation of variable Gr, G/W, H/W, Pr, and B/W was performed using the theoretical model formulated and validated in the foregoing sections. A base set of conditions was defined as $Gr = 10^5$, $G/W = 0.33$, $H/W = 5.0$, $Pr = 0.7$, and $B/W = 1.33$. The dimensionless problem parameters were varied singly about this base case to illustrate the influence of the variables studied. Unless otherwise specified, each of the parameters were maintained at the values prescribed for the base test case.

Normalized vent gap spacing

Enclosures with aspect ratios of 2.5, 5.0, and 10.0 were studied for normalized gap spacings in the range $0.1 \leqslant G/W \leqslant 1.0$. The variation in local Nusselt number along the heated wall for $H/W = 5.0$ and 10.0 is shown in Fig. 3 for $G/W = 0.1$, 0.33, 0.67, and 1.0. The heat transfer from $y/H = 0.2$ to 0.9 is found to be nearly identical for $G/W > 0.33$. However, the local heat transfer profiles near the bottom of the heated wall vary significantly for changing G/W. Note also that Nu is significantly lower in the central region of the enclosure, $0.2 \leqslant y/H \leqslant 0.9$, for the $G/W = 0.1$ configuration. The emergence of local maxima and minima in the Nusselt number is evident, particularly for the $G/W = 0.33$ and 0.67 vent gaps. The unobstructed channel ($G/W = 1.0$) shows the traditional monotonic decay in heat transfer coefficient observed previously [1]. The local heat transfer in the region $0 \leqslant y/H \leqslant 0.3$ was found to be highly nonuniform,

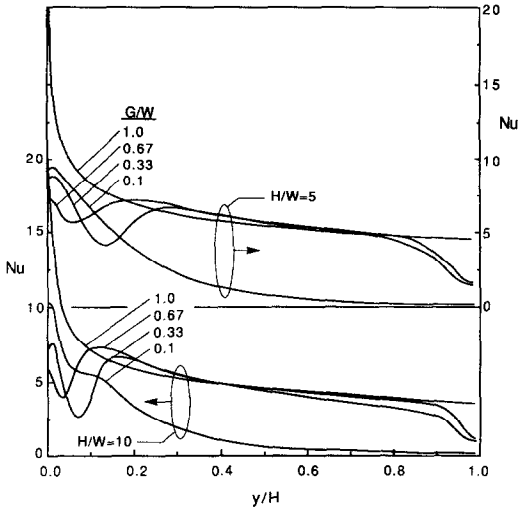

FIG. 3. Influence of dimensionless gap spacing on local Nusselt number along the heated wall for $Pr = 0.7$, $Gr = 10^5$, $H/W = 5.0$ and 10.0.

and will be shown to be dependent on the size of the recirculation zone in the bottom portion of the cavity. The cavity aspect ratio also appears to exercise significant influence on the local heat transfer in the region $y/H \leqslant 0.2$. The difference between local maximum and minimum in Nusselt number is larger for the higher aspect ratio cavity.

The predicted streamline plots shown in Fig. 4 corresponding to the $H/W = 5.0$ local heat transfer data of Fig. 3 illustrate a strong recirculation zone that results from the separation of the inlet flow at the entrance to the cavity. The flow patterns reveal that the structure of the recirculation zone is quite sensitive to the size of the vent opening. The portion of the fluid which is not entrained into the recirculation zone impinges against the heated wall at a point which coincides closely with the location of the locally maximum Nusselt number in Fig. 3. For larger inlet vent gap spacings, a smaller fraction of the inlet fluid is entrained into the recirculation zone. As a result, the amount of fluid passing over the lower-most part of the wall decreases, thus reducing the convective heat transfer at the bottom of the heated surface. The recirculation zone penetrates highest into the enclosure for $G/W = 0.33$. This causes the largest variation in Nu to occur along the lower region of the isothermal wall between $y/H = 0.0$ and 0.2 for this configuration. Note that for the $G/W = 0.10$ configuration much of the fluid drawn into the enclosure forms a growing boundary layer which begins at $y/H = 0$; there is no dominant point of primary flow attachment further up the heated wall as was seen with wider gap spacings. Consequently, the variation in local Nusselt number with vertical position exhibits no pronounced local maximum or minimum. For larger cavity aspect ratios, only a slight inflection in Nu exists where cool inlet fluid is entrained into the boundary layer near $y/H = 0.1$ (see Fig. 3). Although the central portion

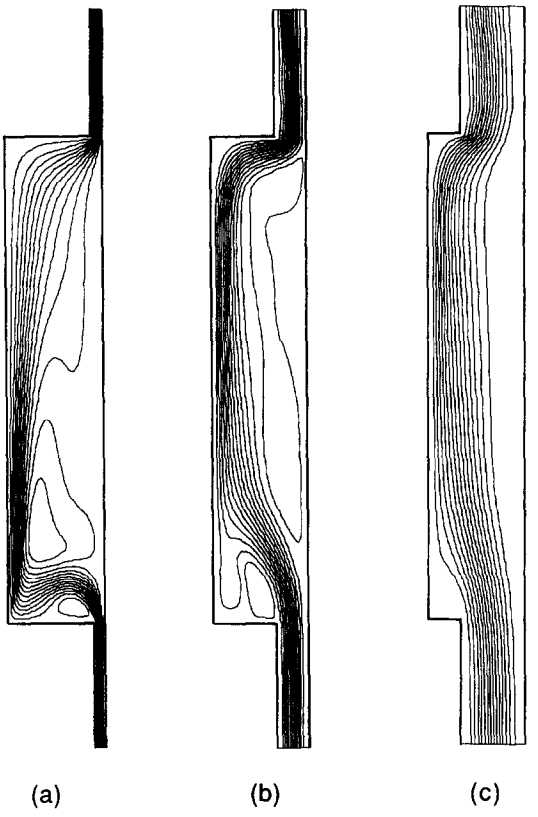

FIG. 4. Predicted flow structure for $H/W = 5.0$, $Gr = 10^5$, $Pr = 0.7$: (a) $G/W = 0.1$; (b) $G/W = 0.33$; (c) $G/W = 0.67$. Streamlines are equi-spaced.

of the enclosure adjacent to the vertical adiabatic boundary is nearly stagnant, a weak downflow is observed in this region.

Figure 5 shows the variation in average Nusselt number with normalized gap spacing for $Gr = 10^5$ and all enclosure aspect ratios studied. The dependence of $\overline{Nu}$ on G/W is quite similar for all H/W studied. The average heat transfer is generally found to increase by about 200% as G/W was increased from 0.10 to 0.33. This is due to the large increase

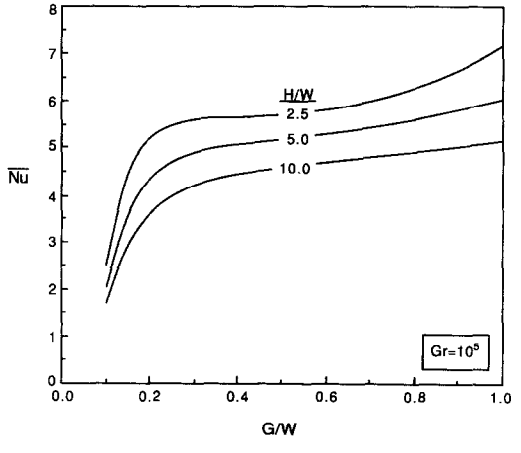

FIG. 5. Variation in average Nusselt number with normalized gap spacing for $Gr = 10^5$, $H/W = 2.5$, 5.0, and 10.0.

observed for the local heat transfer along the upper seven-tenths of the isothermal surface as observed in Fig. 3. It is also seen that a decrease in the cavity aspect ratio is accompanied by a corresponding increase in the average Nusselt number. As will be shown subsequently, the increase in $\overline{Nu}$ between $G/W = 0.1$ and 1.0 is accompanied by a nearly fourfold increase in the induced mass flow.

Examination of the buoyancy-induced average velocity and mass flow rate provides understanding as to the mechanisms for reduction in average heat transfer coefficient for the cavity as a function of normalized gap spacing. The dimensionless flow rate, M^*, may be determined from the average dimensional inlet velocity $\bar{v}_{in}$ according to

$$M^* = \bar{v}_{in} G/\nu. \tag{9}$$

The flow rate may be related to the dimensionless average inlet velocity, $\bar{V}_{in}$, by

$$M^* = \bar{V}_{in}(G/W). \tag{10}$$

The dimensionless mass flow rate M^* resembles a buoyancy induced-flow Reynolds number based on the gap width, G. The dimensionless inlet velocity V_{in} represents an induced-flow Reynolds number based on the enclosure width, W. The predicted dimensionless average velocity and flow rate through the enclosure are illustrated in Fig. 6 for $0.1 \leqslant G/W \leqslant 1.0$ and $H/W = 2.5$, 5.0, and 10.0. The average inlet velocity shows a complex dependence on G/W. $\bar{V}_{in}$ is seen to be relatively low for $G/W = 0.1$, with a significant increase between 0.1 and 0.2. Recall that the average Nusselt number also exhibited substantial increases in the range $0.1 \leqslant G/W \leqslant 0.2$ for all cavity aspect ratios investigated (see Fig. 5). For gap spacings greater than $G/W = 0.2$, the trend is towards decreasing $\bar{V}_{in}$, with the exception of a slight maximum at $G/W = 0.75$ observed primarily in the $H/W = 5.0$ and 10.0 predictions. The maximum at this gap spacing was seen to correspond to a significant collapse in the recirculation zone located in the bottom of the cavity. The variation in mass flow rate shows a monotonic increase for $G/W \leqslant 0.75$. As indicated previously, increases of nearly 400% are observed for the $H/W = 10.0$ configuration. Note the local maximum in M^* for $G/W \approx 0.75$. Again, this is particularly evident in the larger aspect ratio cavities, $H/W = 5.0$ and 10.0. The collapse of the recirculation zone alluded to previously results in a maximum in mass flow rate. Once the inlet flow forms a hydrodynamic boundary layer nearer the bottom of the enclosure, the associated higher frictional forces reduce the flow rate for $G/W \geqslant 0.75$.

Although the dimensionless mass flow increases by nearly 80% between $G/W = 0.33$ and 0.67 for all cavity aspect ratios, only moderate increases in $\overline{Nu}$ are realized for the same increase in gap spacing (Fig. 5). It may be suggested that the majority of the increased flow travels through the enclosure nearer to the adiabatic side wall, which contributes little to the convective heat transfer along the heated surface. This is corroborated by the streamlines of Fig. 4, where the velocity gradient normal to the heated wall is substantially higher for the $G/W = 0.33$ case than for the $G/W = 0.67$ vent gap spacing. Increases in $\overline{Nu}$ are found as G/W is increased to 1.0 because the heat transfer near the bottom and top of the isothermal wall increases due to the elimination of the blockages of flow.

Grashof number

The effects of varying Grashof number were studied over a range extending from 10^2 to $5(10^6)$ for configurations consisting of $H/W = 2.5$ and 5.0, $G/W = 0.33$ and 0.67. Plots of the local Nusselt number as a function of y/H along the isothermal surface for enclosures with $H/W = 5.0$, $G/W = 0.33$, and variable Gr are shown in Fig. 7. Grashof numbers below 10^3 yield smooth local heat transfer profiles instead of the highly non-uniform patterns observed for larger Grashof numbers along the lower section of the heated surface. The profiles were nearly identical for

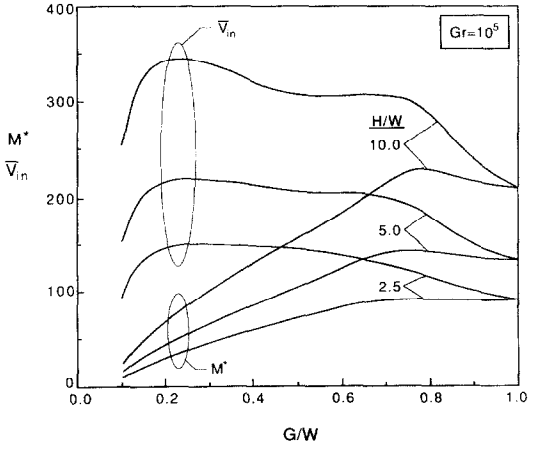

FIG. 6. Predicted variation of dimensionless average inlet velocity and induced flow rate with gap spacing and aspect ratio for $Gr = 10^5$, $Pr = 0.7$.

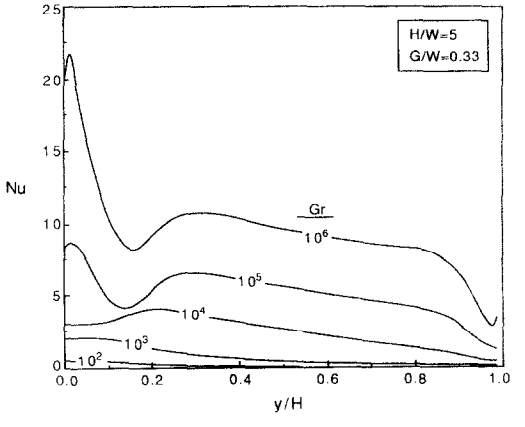

FIG. 7. Variation of the local Nusselt number with Grashof number for $H/W = 5.0$, $G/W = 0.33$, $Pr = 0.7$.

$Gr = 10^2$ and 10^3. Conduction is the principal mode of heat transfer for these cases since the driving force for convection is small. As Gr is increased, the relative buoyancy forces increase and Nu rises.

As Gr is increased to 10^4, the heat transfer profiles form a type of hump shape with a local maximum near $y/H = 0.2$ This suggests that only a very weak recirculation zone is predicted to occur near the lower wall for $Gr = 10^4$ for the enclosure with $H/W = 5.0$, $G/W = 0.33$. This resulted in the smooth profiles for the local Nusselt number for this value of Gr. The non-uniform Nu profile over the lower region of the heated wall for $Gr \leqslant 10^5$ suggests that the strength of the recirculation zone significantly increases with larger Grashof numbers.

Figure 8 illustrates the predicted average Nusselt number variation with Grashof number for all configurations studied. Also shown in the figure is the correlation for the limiting case of $G/W = 1.0$ [2]. This limiting condition constitutes an unobstructed vertical parallel plate channel heated asymmetrically. The correlation is given as

$$\overline{Nu} = \left[\frac{144}{(Ra\,W/H)^2} + \frac{2.8}{(Ra\,W/H)^{1/2}}\right]^{-1/2}. \quad (11)$$

A general increase in $\overline{Nu}$ is seen for increasing values of Gr. The figure indicates that flow destabilization occurs at approximately $Gr = 10^3$. The critical Grashof number at which buoyancy becomes important is increased for larger aspect ratio enclosures, but is seen to be only weakly dependent on vent gap spacing. As seen by the slopes of the $\overline{Nu}$–Gr lines, the predictions asymptote to an approximate average Nusselt number dependence $\overline{Nu} \sim Gr^{1/4}$, regardless of gap spacing. Only the magnitude of the average heat transfer is reduced by the presence of the blockage at the inlet and exit. The dependence of the Nusselt number on $Gr^{1/4}$ is suggested by the limiting configuration $G/W = 1.0$, $H/W \to \infty$ corresponding to free convection from an isolated, isothermal plate [16].

The increased buoyancy force relative to the viscous forces which occurs at higher Grashof number raises the velocities of the convecting medium and subsequently the local and average heat transfer. The magnitude of the induced mass flow in the enclosure was seen to behave similarly to $\overline{Nu}$ (not shown). The dimensionless mass flow was seen to increase by approximately two orders of magnitude for an increase in Grashof number from 10^3 to 10^6, regardless of gap spacing [15].

Aspect ratio

Enclosures with aspect ratio $H/W = 1.0$, 2.5, 5.0, and 10.0 were investigated for $G/W = 0.10$, 0.33, and 0.67. Figure 9 illustrates the variation of local Nusselt number with position along the heated wall for variable aspect ratios with $G/W = 0.33$. Of the gap spacings analyzed, $G/W = 0.33$ yielded the most irregular Nu profiles along the bottom half of the enclosure. Each of the configurations for this gap spacing, except $H/W = 1.0$, exhibited a well-defined peak and valley in the Nu profile [15]. The difference between the local maximum and the local minimum was largest for $H/W = 10.0$; a nearly twofold increase in Nu was observed between $y/H = 0.1$ and 0.2.

For smaller values of H/W, the relative height of the enclosure is smaller. Hence, it is believed that the primary inlet flow attaches to the heated surface at a larger value of y/H. This would tend to increase the value of y/H where the peak and valleys in the profiles occur which may also be seen in Figure 9. The magnitude of the local maximum and minimum in the Nu profile was also found to be dependent on aspect ratio. As H/W is increased, the relative difference in the magnitudes of the peaks and valleys increase; Nu_{min} decreases by nearly 45% as H/W is increased from 2.5 to 10.0. This is due to the increased chimney effect brought on by the larger relative height of the heated wall. For $H/W = 10.0$, the stronger buoyancy force does not allow the primary inlet air to flow around the recirculation zone and penetrate the region of the heated wall below $y/H \approx 0.15$. This results in a lower local minimum alongside the recirculation zone

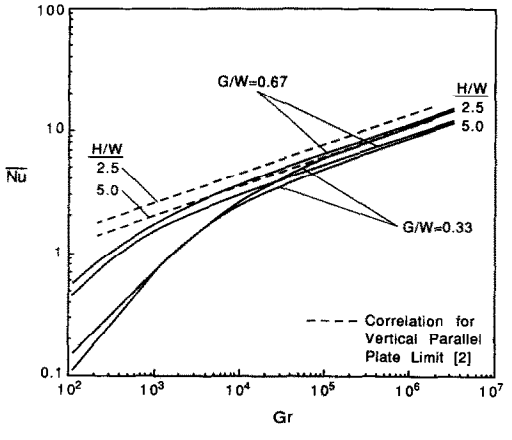

FIG. 8. Dependence of the average Nusselt number on Grashof number for all configurations studied, $Pr = 0.7$.

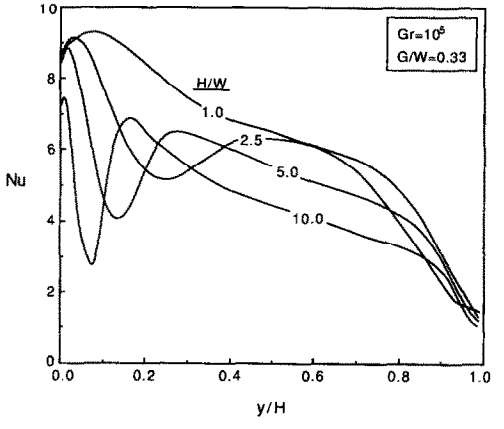

FIG. 9. Profiles of local Nusselt number for various aspect ratios investigated, $Gr = 10^5$, $G/W = 0.33$, $Pr = 0.7$.

and a sharp increase in Nu where the majority of the primary inlet attaches to the wall.

The effect of the recirculation zone on the local heat transfer is reduced for decreasing aspect ratio; the smaller buoyancy force allows the primary inlet air to flow around the recirculation zone and attach lower on the heated wall. The difference between the magnitudes of the local minimum and maximum heat transfer is therefore reduced for smaller aspect ratios. The magnitude of the local maximum remains relatively constant. However, the Nu_{min} increases as H/W is decreased. Hence, the strong variation in local Nusselt number in the lower portion of the enclosure diminishes for decreasing H/W. For $H/W = 1.0$, the local minimum (valley) in the heat transfer profile vanishes. In addition, the locations of the peaks and valleys of the profiles shift up the wall toward the exit for decreasing aspect ratio. The local Nusselt number decreases monotonically for each configuration along the upper half of the heated wall.

The plot of $\overline{Nu}$ vs H/W included in Fig. 10 shows that $\overline{Nu}$ decreases as H/W increases. The larger relative height of the heated wall (large H/W) allows the thermal boundary layer to continue to thicken and hence, increase the resistance to heat transfer. The most rapid decline in $\overline{Nu}$ is evident for $G/W = 0.10$. The value of $\overline{Nu}$ decreases by 28% as H/W increases from 1.0 to 10.0. For a similar increase in H/W, the average Nusselt number decreases by 13 and 7% for $G/W = 0.33$ and 0.67, respectively. The largest decrease in the average heat transfer occurs at $G/W = 0.10$ because the majority of the inlet fluid attaches to the heated wall at $y/H = 0$. As a result, the thermal boundary layer continues to grow from this point. Comparison with the Nusselt number correlation for the unobstructed ($G/W = 1.0$) configuration [2] clearly shows the reduction in $\overline{Nu}$ with decreasing G/W, as well as the same general decreasing trend with cavity aspect ratio, H/W.

Prandtl number

An enclosure consisting of $H/W = 5.0$, $G/W = 0.33$ for Gr ranging from 10^2 to $5(10^6)$ was used to study the effect of variable Prandtl number for $Pr = 0.7$, 5, and 20. The local heat transfer profiles for $Gr = 10^5$ and variable Pr are shown in Fig. 11. Study of this figure reveals that significant changes are evident in both the shape and magnitude of the Nu profiles for varying Prandtl number. The relative increase in local Nusselt number for higher Prandtl number fluids is an artifact of their generally lower thermal conductivity. As Pr is increased from 0.7 to 5 the non-uniform local heat transfer pattern between $y/H = 0.0$ and 0.3 is eliminated. Instead of a peak and valley in the local heat transfer profile, the local Nusselt number decreases nearly monotonically for $Pr = 5$ and 20. The absence of maxima and minima in the local Nusselt number for higher Prandtl number fluids may be explained by the relative thicknesses of the thermal and hydrodynamic boundary layers. The ratio of the thermal to hydrodynamic boundary layer thickness is much lower for the $Pr = 20$ fluid and hence, the local heat transfer is coupled less intimately to the flow structure. Thus, the recirculation in the lower part of the cavity and point of primary flow attachment exert less influence on the local heat transfer. The influence of the Prandtl number on average Nusselt number was found to correlate reasonably well if the Rayleigh number was used in lieu of the Grashof number [15].

Normalized vent length

The length of the inlet and exit vents was the last parameter investigated, and the findings are summarized here. Enclosures consisting of $H/W = 5.0$, $G/W = 0.33$; $H/W = 5.0$, $G/W = 0.67$; and $H/W = 2.5$, $G/W = 0.67$ were considered for $B/W = 1.0$, 5.0, and 10.0. The average heat transfer predictions for these configurations revealed that little change in the heat transfer occurs as B/W is increased from 1.0 to 10.0 for $G/W = 0.33$; the average Nusselt number was seen to decrease by nearly 10% for B/W increasing from 1.0 to 10.0. Interestingly, this is accompanied by a nearly 50% increase in the induced flow rate. An increase in B/W increases the unheated exit length and hence, the buoyancy force in the

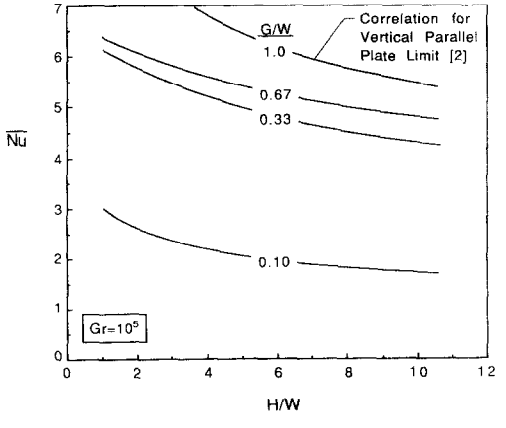

FIG. 10. Variation of average Nusselt number with cavity aspect ratio, $Gr = 10^5$, $Pr = 0.7$.

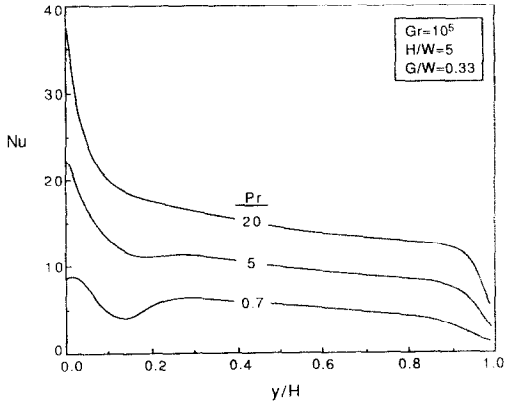

FIG. 11. Profiles of the local Nusselt number for $Gr = 10^5$, $H/W = 5.0$, and $G/W = 0.33$ for $Pr = 0.7$, 5, and 20.

system. The result is higher mass flow rate. A complete discussion of vent gap effects may be found elsewhere [15].

Correlation of average Nusselt number

Correlations of the numerical data using multiple linear regression polynomials were made to quantify the dependence of the average Nusselt number on the Grashof number, gap spacing, and Prandtl number. It was not possible to develop correlations which examined the effects of aspect ratio and vent length because of the lack of data for these parameters. Correlations are presented for $H/W = 5.0$ and $B/W = 1.33$. It has been shown, however, that the average heat transfer was relatively insensitive to changes in B/W.

The average Nusselt number may be correlated as a function of Grashof number, dimensionless gap spacing, and fluid Prandtl number using the relation

$$\overline{Nu} = 0.33 Gr^{0.261} (G/W)^{0.175} Pr^{0.345}. \quad (12)$$

Equation (12) was found to represent the predicted average Nusselt number variation with an average error of 4% for all simulations performed. The correlation is valid for $H/W = 5.0$ and $B/W = 1.33$ in the respective ranges $0.33 \leqslant G/W \leqslant 1.0$, $10^4 \leqslant Gr \leqslant 10^7$, and $0.7 \leqslant Pr \leqslant 20$. It was not possible to correlate the data for $G/W = 0.1$.

The correlation was compared to the empirical equation developed by Bar-Cohen and Rohsenow [2] for a parallel-plate, vertical channel with one isothermal wall and one adiabatic wall, given by equation (11). Recall that the vertical channel resembles the vented enclosure in the limit of $G/W = 1.0$. Therefore, the correlated average Nusselt numbers for $G/W = 1.0$ were expected to be similar to those predicted by equation (11). Over the applicable range of parameters for $H/W = 5.0$ it was found that the correlation differed from the predicted data represented by equation (12) by an average of 7%. A possible cause for the slight discrepancies observed in the correlations is the unheated inlet and exit vent lengths present for the vertically vented enclosure even though $G/W = 1.0$.

CONCLUSIONS

Buoyancy driven flow and heat transfer in a vertically-vented enclosure has been investigated numerically. After validation of the model, the effects of the normalized vent gap spacing, enclosure aspect ratio, Grashof number, and Prandtl number on the flow structure and local and average heat transfer were examined. A complex flow pattern which includes a large recirculation zone near the inlet vent was found to be highly dependent on the gap spacing. The local heat transfer was discovered to be very nonuniform along the lower half of the heated wall as a result of the recirculating flow structure. The predictions for the flow field reveal that the local variations in heat transfer in this region are attributed to the complex flow patterns in the lower half of the cavity, which are strongly dependent on the vent gap. The results show asymptotic behavior to the classical vertical parallel plate result in the limit as the vent gap approaches the enclosure width.

Acknowledgement—Financial support of this work under U.S. National Science Foundation Grant CBT-8552493 is gratefully acknowledged. Helpful discussions with Prof. S. Ramadhyani are also appreciated.

REFERENCES

1. W. Aung, L. S. Fletcher and V. Sernas, Developing laminar free convection between vertical plates with asymmetric heating, *Int. J. Heat Mass Transfer* **16,** 2293–2308 (1972).
2. A. Bar-Cohen and W. M. Rohsenow, Thermally optimum spacing of vertical natural convection cooled, parallel plates, *ASME J. Heat Transfer* **106,** 116–123 (1984).
3. E. M. Sparrow, G. M. Chrysler and L. F. Azevedo, Observed flow reversals and measured-predicted Nusselt numbers for natural convection in a one-sided heated vertical channel, *ASME J. Heat Transfer* **106,** 325–332 (1984).
4. B. Gebhart, Y. Jaluria, R. L. Mahajan and B. Sammakia, *Buoyancy-induced Flows and Transport.* Hemisphere, New York (1988).
5. F. Penot, Numerical calculation of two-dimensional natural convection in isothermal open cavities, *Numer. Heat Transfer* **5,** 421–437 (1982).
6. C. F. Hess and R. H. Henze, Experimental investigation of natural convection losses from open cavities, *ASME J. Heat Transfer* **106,** 333–338 (1984).
7. Y. L. Chan and C. L. Tien, A numerical study of two-dimensional natural convection in square open cavities, *Numer. Heat Transfer* **8,** 65–80 (1985).
8. Y. L. Chan and C. L. Tien, Laminar natural convection in shallow open cavities, *ASME J. Heat Transfer* **108,** 305–309 (1986).
9. J. A. C. Humphrey and W. M. To, Numerical simulation of buoyant, turbulent flow, Part 2. Free and mixed convection in a heated cavity, *Int. J. Heat Mass Transfer* **29,** 593–610 (1986).
10. A. M. Clausing, J. M. Waldvogel and L. D. Lister, Natural convection from isothermal cubical cavities with a variety of side-facing apertures, *ASME J. Heat Transfer* **109,** 407–412 (1987).
11. M. Miyamoto, T. H. Kuehn, R. J. Goldstein and Y. Katoh, Two-dimensional laminar natural convection heat transfer from a fully or partially open square cavity, *Numer. Heat Transfer*, Part A **15,** 411–430 (1989).
12. T. Aihara, Effects of inlet boundary conditions on numerical solutions of free convection between vertical parallel plates, Report of the Institute of High Speed Mechanics, Vol. 28, pp. 1–27 (1973).
13. P. R. Chappidi and B. E. Eno, A comparative study of the effect of inlet conditions on a free convection flow in a vertical channel, *ASME J. Heat Transfer* **112,** 1082–1085 (1990).
14. S. V. Patankar, *Numerical Heat Transfer and Fluid Flow.* McGraw-Hill, New York (1980).
15. D. M. Sefcik, Natural convection heat transfer in a vertically-vented enclosure, M.S. Thesis, Department of Mechanical Engineering, Brigham Young University, Provo, Utah (1990).
16. S. Ostrach, An analysis of laminar free convection flow and heat transfer about a flat plate parallel to the direction of the generating body force, National Advisory Committee for Aeronautics, Report 111 (1953).

ANALYSE DE LA CONVECTION NATURELLE DANS DES ENCEINTES VERTICALEMENT VENTILEES

Résumé—On étudie théoriquement la convection naturelle dans des cavités ventilées verticalement. Une telle cavité est telle que l'écoulement flottant et le transfert de chaleur sont conditionnés par des évents au sommet et au plancher des parois de la cavité. Les équations de conservation sont résolues numériquement par une technique de volume de contrôle et de différences finies avec les conditions aux limites de pression appropriées aux évents. Les résultats révèlent un transfert thermique local non uniforme le long des parois isothermes du fait de blocage à l'entrée. Un maximum local et un minimum du transfert thermique apparaissent dans la moitié inférieure de la cavité. Les prédictions du champ d'écoulement révèlent que ces extrema sont attribuables à une zone de recirculation proche de l'évent d'entrée et au recollement de l'écoulement primaire le long de la paroi chauffée. Les résultats montrent un comportement asymptotique au cas classique des plaques verticales parallèles lorsque la largeur de l'évent d'entrée s'approche de celle de la cavité.

ANALYSE DES WÄRMEÜBERGANGS DURCH NATÜRLICHE KONVEKTION IN SENKRECHT BELÜFTETEN HOHLRÄUMEN

Zusammenfassung—Die natürliche Konvektion in senkrecht belüfteten Hohlräumen wird theoretisch untersucht. Ein senkrecht belüfteter Hohlraum ist dadurch gekennzeichnet, daß die Auftriebsströmung und der Wärmeübergang durch Lüftungsschlitze an der oberen und unteren Stirnwand beeinflußt werden. Die grundlegenden Erhaltungsgleichungen werden unter Verwendung eines Finite-Differenzen-Verfahrens mit Kontrollvolumina numerisch gelöst. Dabei werden an den unteren und oberen Lüftungsschlitzen geeignete Randbedingungen für den Druck eingesetzt. Es zeigt sich, daß der örtliche Wärmeübergang entlang der isothermen Wände aufgrund der Behinderung am Einlaß stark ungleichförmig ist. In der unteren Hälfte des Hohlraums weist der Wärmeübergang ein örtliches Maximum und Minimum auf. Die Berechnung des Strömungsfeldes zeigt, daß diese Extrema durch eine Rezirkulationszone in der Nähe des Einlaßschlitzes hervorgerufen werden, wodurch sich die Primärströmung an die beheizte Wand anlegt. Die Ergebnisse zeigen ein asymptotisches Verhalten hin zum klassischen Ergebnis für die senkrechten parallelen Platten. Dieser Grenzfall wird dann erreicht, wenn die Breite des Lüftungsschlitzes diejenige des Hohlraums erreicht.

АНАЛИЗ ЕСТЕСТВЕННОЙ КОНВЕКЦИИ В ВЕРТИКАЛЬНЫХ ПРОТОЧНЫХ ПОЛОСТЯХ

Аннотация—Теоретически исследуется естественная конвекция в проточных полостях. Теплоперенос и гравитационное течение исследуются в полости, ограниченной отверстиями в верхней и нижней стенках. Уравнения сохранения решаются численно с использованием конечно-разностной схемы методом контрольных объемов при соответствующих граничных условиях для давления во входном и выходном отверстиях. Полученные результаты показывают, что наличие отверстий вызывает существенно неоднородный локальный теплоперенос вдоль изотермической стенки. Локальные максимум и минимум теплопереноса наблюдаются в нижней части полости. Расчеты поля течения свидетельствуют о том, что указанные экстремальные значения связаны с наличием рециркуляционной зоны вблизи входного отверстия и основного течения у нагретой стенки. Результаты показывают, что решение асимптотически стремится к классическому случаю вертикальной параллельной пластины, когда размер отверстия приближается к ширине полости.